AIMS Mathematics, 8(8): 19677–19698.
DOI: 10.3934/math.20231003
Received: 07 January 2023
Revised: 24 April 2023
Accepted: 24 April 2023
Published: 12 June 2023

http://www.aimspress.com/journal/Math

Research article

A meshless method for numerical solutions of linear and nonlinear time-fractional Black-Scholes models

Hijaz Ahmad[1,2,3,*], **Muhammad Nawaz Khan**[4], **Imtiaz Ahmad**[5], **Mohamed Omri**[6] **and Maged F. Alotaibi**[7]

[1] Near East University, Operational Research Center in Healthcare, Nicosia, 99138, TRNC Mersin 10, Turkey

[2] Department of Computer Science and Mathematics, Lebanese American University, Beirut, Lebanon

[3] Section of Mathematics, International Telematic University Uninettuno, Corso Vittorio Emanuele II, 3900186, Roma, Italy

[4] Department of Basic Sciences, University of Engineering and Technology Peshawar, Pakistan

[5] Institute of Informatics and Computing in Energy (IICE), Universiti Tenaga Nasional, Kajang, Selangor, Malaysia

[6] Deanship of Scientific Research, King Abdulaziz University, Jeddah, Saudi Arabia

[7] Department of Physics, College of Science, King Abdulaziz University, Jeddah, Saudi Arabia

* **Correspondence:** Email: hijaz555@gmail.com.

Abstract: The numerical solution of the time-fractional Black-Scholes model for European and American options is presented using a local meshless collocation approach based on hybrid Gaussian-cubic radial basis functions with polynomials is presented. The approach is then expanded to a nonlinear time-fractional model for an option with transaction costs in a market with low liquidity. The spatial derivatives of the models are discretized using the proposed meshless technique. Numerical experiments are carried out for the American option, European option, and nonlinear transaction cost option models. In order to evaluate the effectiveness and precision of the suggested meshless approach, L_∞ and L_{rel} error norms are utilized. Both call and put option volatility is explored. A non-uniform grid customized around the strike price region is also used to determine the prices of European call and American put options. The methods described in literature are compared with the numerical results.

Keywords: time-fractional Black-Scholes model; hybrid local meshless method; radial basis functions; polynomial
Mathematics Subject Classification: 26A33, 65D12, 91G20

1. Introduction

In financial investment, one of the popular and significant components of financial derivatives is the stock option. In view of both theory and practice, option pricing mathematical palatial differential equation (PDE) models constitute an important subject to be explored beyond integer order. Black and Scholes [1] constructed a model in the form of second-order parabolic integer order PDEs with respect to stock price and time. This model is based on geometric Brownian motion with a constant drift and volatility. However, due to the idealistic standards of the traditional Black-Scholes (BS) model, integer order PDEs may not effectively simulate the process in situations with hops over small time steps to capture the substantial fluctuations of a stock price [2]. With the newfound features of the fractional PDEs, the fractional BS equations appear more relevant to extend mathematical models related to option pricing.

When a fractional order PDE is used for the financial modelling, the involved standard Brownian motion in the stochastic process of the classical model is replaced by fractional Brownian motion. The non-locality of integrals and fractional derivatives is a powerful resource for memory illustration [3]. Jumarie [4] applied the fractional Taylor formula to derive the time- and space-fractional BS models. To price the exotic options in markets with jumps, a fractional diffusion model was developed by Cartea and del-Castillo-Negrete [5]. Liang et al. [6] proposed bifractional BS models of option pricing. Farhadi et al. [3] employed a time-fractional BS model (TFBSM) to describe the effect of trend memory. Considering the rising challenges involved in obtaining the solution of more complex fractional BS PDEs models, further investigation into the subject seems to be a very important and practical research objective.

To price the European option price using the fractional BS model, Zhang et al. [7] utilized implicit finite difference techniques and Özdemir and Yavuz [8] used multivariate Padé approximation; Cen et al. [9] used an integral discretization scheme for time and for the spatial discretization, the central differencing scheme (CDM) on a piecewise uniform mesh was used.

To solve the American option fractional BS model, Chen [10] employed a predictor-corrector approach in a finite-moment log-stable model. To investigate a space-fractional parabolic variational inequality model for pricing American options, a power penalty method with a finite-difference mechanism was utilized by Chen and Wang [11]. Without costs on the transactions of risky and riskless securities, the BS model has been an effective procedure for pricing options in a complete market. However, the BS option pricing methodology is not useful for riskless securities or stocks in the presence of transaction costs on trading, as it is impossible to perfectly hedge [12]. Edeki et al. [13] has extended the nonlinear BS model to time-fractional order and utilized a modified differential transform method for numerical solution of the model. In recent years, physics-informed neural networks have emerged as a popular meshless method for solving the BS model and forward and inverse PDE problems [14, 15].

For the solutions of several types of challenging linear, nonlinear, integer- and fractional-order PDEs that arise in science and engineering [16–19], meshless methods using radial basis functions (RBFs) represent a feasible alternative numerical mechanism. In the literature, various meshless techniques have been published. The reported work includes the Piret and Hanert [20] fractional diffusion equations, Hosseini et al. [21] fractional telegraph equation, Ghehsareh et al. [22] two-dimensional fractional evolution equation, Kumar et al. [23] time-fractional diffusion wave

equation, Dehghan et al. [24] time-fractional nonlinear sine-Gordon and Klein-Gordon equations Mohebbi et al. [25] time-fractional nonlinear Schrödinger equation, Mohebbi et al. [26] two-dimensional modified anomalous fractional sub-diffusion equation, Wei et al. [27] two-dimensional time-fractional diffusion equations, Aslefallah and Shivanian [28] nonlinear time-fractional integro-differential reaction-diffusion equation, Wei et al. [29] variable-order time-fractional diffusion equation and Avazzadeh et al. [30] time-fractional diffusion-wave equation.

Very few authors have attempted to solve the TFBSM by using an RBF to price the European option [31]. To the best of our knowledge, this article is the first one to extend the local RBFs collocation method (LRBFCM) to solve the TFBSM with American options and nonlinear TFBSM with transaction cost in an illiquid market. In this paper, a hybrid Guassian-cubic RBF [32] is first localized and then appended with a linear polynomial in order to reduce the ill-conditioned problem of the resultant coefficient matrix. Afterward, by utilizing the localized hybrid RBF method, the solution of the time-fractional BS model can be computed accurately and efficiently, while also preserving the maximum principle. This method has the potential to be applied to different variants of fractional BS models, other PDE problems in finance and other fields that involve fractional derivatives.

The proposed LRBFCM improves the accuracy and stability of function approximation by combining a low-degree polynomial component with an RBF component. The polynomial component captures the overall behavior of the function, while the RBF component focuses on the local features. This hybrid approach is more effective than traditional RBF methods as it can capture both local and global features of the function.

2. Preliminaries and models

Definition 2.1. The right modified Riemann-Liouville derivative [4, 33] is

$$\frac{\partial^\beta p(v,\tau)}{\partial \tau^\beta} = \frac{1}{\Gamma(1-\beta)} \frac{d}{d\tau} \int_\tau^T \frac{(p(v,\zeta) - p(v,T))}{(\zeta-\tau)^\beta} d\zeta, \quad 0 < \beta \le 1. \tag{2.1}$$

Definition 2.2. The Caputo's fractional derivative [34] is

$$\frac{\partial^\beta p(v,\tau)}{\partial \tau^\beta} = \frac{1}{\Gamma(1-\beta)} \int_0^\tau (\tau-\zeta)^{-\beta} p_\zeta(v,\zeta) d\zeta, \quad 0 < \beta \le 1. \tag{2.2}$$

The TFBSM [7, 35] for option pricing along with the boundary and final conditions is

$$\begin{aligned} &\frac{\partial^\beta p}{\partial \tau^\beta} = -\frac{1}{2}\sigma^2 v^2 \frac{\partial^2 p}{\partial v^2} - rv\frac{\partial p}{\partial v} + rp, \quad 0 < \beta \le 1, 0 \le \tau \le T, v \ge 0, \\ &p(0,\tau) = g_1(\tau), \quad p(+\infty,\tau) = g_2(\tau), \\ &p(v,T) = v(v). \end{aligned} \tag{2.3}$$

The basic assumption of model (2.3) is that the underlying asset follows the standard geometric Brownian motion pattern and that variation in option price is similar to fractal transmission [7, 35]. A

linear transformation of the variable $t = T - \tau$ converts model (2.3) to an initial value problem with the payoff function as an initial condition. Thus, a reformulated fractional PDE model along with its boundary and initial conditions is

$$\begin{aligned} &\frac{\partial^\beta p}{\partial t^\beta} = \frac{1}{2}\sigma^2 v^2 \frac{\partial^2 p}{\partial v^2} + rv\frac{\partial p}{\partial v} - rp, \\ &p(0,t) = g_1(t), \quad p(+\infty, t) = g_2(t), \\ &p(v,0) = v(v). \end{aligned} \tag{2.4}$$

Equation (2.4) reduces to a classical BS model for $\beta = 1$. Specifically, the following three models are considered for derivation of the numerical solution via the proposed mechanism.
(*i*). The TFBSM for European options [36]

$$\begin{aligned} &\frac{\partial^\beta p}{\partial t^\beta} - \frac{1}{2}\sigma^2 v^2 \frac{\partial^2 p}{\partial v^2} - rv\frac{\partial p}{\partial v} + rp = 0, \quad (v,t) \in (0, v_{max}) \times (0,T), \\ &p(0,t) = g_1(t), \quad p(v_{max}, t) = g_2(t), \\ &p(v,0) = v(v). \end{aligned} \tag{2.5}$$

(*ii*). The nonlinear TFBSM in an illiquid market with transaction costs [13]

$$\frac{\partial^\beta p}{\partial t^\beta} + rv\frac{\partial p}{\partial v} + \frac{1}{2}\sigma^2 v^2 \left(1 + 2\rho v \frac{\partial^2 p}{\partial v^2}\right)\frac{\partial^2 p}{\partial v^2} - rp = 0, \quad (v,t) \in (0, v_{max}) \times (0,T), \tag{2.6}$$

subject to

$$p(v,0) = \max\left(v - \rho^{-1}\left(\sqrt{v_o v + \frac{v_o}{4}}\right), 0\right).$$

(*iii*). The TFBSM for American put options using the penalty term approach [37]. The following form is the extension of the model in [38, 39] on a fixed domain to time-fractional order.

$$\begin{aligned} &\frac{\partial^\beta p}{\partial t^\beta} = \frac{1}{2}\sigma^2 v^2 \frac{\partial^2 p}{\partial v^2} + rv\frac{\partial p}{\partial v} - rp + \frac{\mu C}{p + \mu - q(v)}, \quad (v,t) \in (0, v_{max}) \times (0,T), \\ &p(v,0) = \max(E - v, 0), \\ &p(0,t) = E, \quad \lim_{v \to \infty} p(v,t) = 0, \end{aligned} \tag{2.7}$$

where $0 < \beta \leq 1$, the stock price is v, the initial stock price is v_o, $\sigma(\geq 0)$ is the volatility of the returns, r is the risk-free rate, the strike price is E, the expiry time is T, the liquidity of the market is ρ, $C \geq rE$, $0 < \mu \ll 1$, $q(v) = E - v$ and the price of the option is $p(v,t)$.

3. Space derivatives discretization using the LRBFCM

The derivatives of $p(v,t)$ are approximated at the centers v_i, $\{v_{i_1}, v_{i_2}, v_{i_3}, ..., v_{i_{n_i}}\} \subset \{v_1, v_2, \ldots, v_{N^n}\}, n_i \ll N^n, i = 1, 2, \ldots, N^n$.

$$p(v_i) \approx \sum_{j=1}^{n_i} \lambda_j \psi(v_{ij}) + \sum_{j=1}^{n_i} \gamma_k p(v_{ij}),\ i = 1, 2, \ldots, N, \tag{3.1}$$

where ψ is a hybrid RBF, $\psi(\|v_{ij} - v_l\|) = \exp\left(-\|v_{ij} - v_l\|^2/c^2\right) + \omega\|v_{ij} - v_l\|^3$, $l = i_1, i_2, \ldots, i_{n_i}$, $p(v_{ij})$ is a linear combination of polynomials on $\mathbb{R}^d$, the shape parameter is c and $\omega = 10e^{-6}$ along with the following extra consistency conditions

$$\sum_{j=1}^{n_i} \lambda_j p(v_{ij}) = 0,\ i = 1, 2, \ldots, N. \tag{3.2}$$

The matrix form of (3.1) and (3.2) is

$$\begin{bmatrix} \boldsymbol{p} \\ 0 \end{bmatrix} = \begin{bmatrix} B & P \\ P^T & 0 \end{bmatrix} \begin{bmatrix} \boldsymbol{\lambda} \\ \boldsymbol{\gamma} \end{bmatrix}, \tag{3.3}$$

where $\boldsymbol{p} = [p_{i_1}, \cdots, p_{i_{n_i}}]^T$, $B = \psi(\|v_{ij} - v_l\|)$, $\boldsymbol{\lambda} = [\lambda_{i_1}, \cdots, \lambda_{i_{n_i}}]^T$, $\boldsymbol{\gamma} = [\gamma_{i_1}, \cdots, \gamma_{i_{n_i}}]^T$ and $P = p(v_{ij})$. The matrix form of (3.3) is

$$\mathfrak{P} = \mathbb{B}\boldsymbol{\Lambda}, \tag{3.4}$$

where $\boldsymbol{\Lambda} = \begin{bmatrix} \boldsymbol{\lambda} \\ \boldsymbol{\gamma} \end{bmatrix}$, $\mathbb{B} = \begin{bmatrix} B & P \\ P^T & 0 \end{bmatrix}$ and $\mathfrak{P} = \begin{bmatrix} \boldsymbol{p} \\ 0 \end{bmatrix}$.

The matrix $\mathbb{B}$ invertibility is ensured by [40]. From (3.4), we have

$$\boldsymbol{\Lambda} = \mathbb{B}^{-1}\mathfrak{P}. \tag{3.5}$$

Differentiating (3.1) yields the derivative of p

$$p^{(m)}(v_i) = \sum_{j=1}^{n_i} \lambda_j \phi^{(m)} + \sum_{j=1}^{n_i} \gamma_j p^{(m)},\ i = 1, 2, \ldots, N. \tag{3.6}$$

The matrix notation of (3.6) is

$$\mathfrak{P}^{(m)} = \mathbb{B}^{(m)}\boldsymbol{\Lambda}, \tag{3.7}$$

or

$$\mathfrak{P}^{(m)} = \mathbb{B}^{(m)}\mathbb{B}^{-1}\mathfrak{P}. \tag{3.8}$$

The approximate semi-discretized LRBFCM form along with the initial conditions, and boundary conditions is given for models (2.5)–(2.7)

$$\frac{d^\beta \mathfrak{p}}{dt^\beta} = \mathcal{D}\mathfrak{p} + \mathbf{k}(t),\ \mathfrak{p}(0) = \mathbf{b}, \tag{3.9}$$

where the LRBFCM approximation yields $\mathcal{D}$ as the sparse coefficient matrix. The order of vectors $\mathbf{b}$ and $\mathbf{k}$ is $N \times 1$ and the vectors $\mathbf{b}$ and $\mathbf{k}$ denote the initial and boundary conditions of the problem respectively.

4. Time derivative discretization

Caputo's time derivative $\frac{\partial^\beta p(v,t)}{\partial t^\beta}$ for $0 < \beta \leq 1$ is

$$\frac{\partial^\beta p(v,t)}{\partial t^\beta} = \begin{cases} \frac{1}{\Gamma(1-\beta)} \int_0^t \frac{\partial p(v,\eta)}{\partial \eta} (t-\eta)^{-\beta} d\eta, & 0 < \beta < 1 \\ \frac{\partial p(v,t)}{\partial t}, & \beta = 1. \end{cases} \tag{4.1}$$

Consider $M+1$ equally spaced time steps $t_0, t_1, \ldots, t_M$ in the interval $[0, t]$, such that the time steps τ, $t_n = n\Im$, $n = 0, 1, 2, \ldots, M$, and that the first-order finite difference scheme to approximate time-fractional derivative term is

$$\begin{aligned}\frac{\partial^\beta p(v, t_{n+1})}{\partial t^\beta} &= \frac{1}{\Gamma(1-\beta)} \int_0^{t_{n+1}} \frac{\partial p(v,\eta)}{\partial \eta} (t_{n+1} - \eta)^{-\beta} \, d\eta, \\ &= \frac{1}{\Gamma(1-\beta)} \sum_{j=0}^{n} \int_{j\Im}^{(j+1)\Im} \frac{\partial p(v,\eta_j)}{\partial \eta} \left(t_{j+1} - \eta\right)^{-\beta} d\eta,\end{aligned} \tag{4.2}$$

where $\frac{\partial p(v,\eta_j)}{\partial \eta}$ is approximated as follows

$$\frac{\partial p(v,\eta_j)}{\partial \eta} = \frac{p(v,\eta_{j+1}) - p(v,\eta_j)}{\eta} + O(\Im).$$

Then

$$\begin{aligned}\frac{\partial^\beta p(v, t_{n+1})}{\partial t^\beta} &= \frac{1}{\Gamma(1-\beta)} \sum_{j=0}^{n} \frac{p(v,t_{j+1}) - p(v,t_j)}{\Im} \int_{j\Im}^{(j+1)\Im} \left(t_{j+1} - \eta\right)^{-\beta} d\eta, \\ &= \frac{1}{\Gamma(1-\beta)} \sum_{j=0}^{n} \frac{p(v,t_{n+1-j}) - p(v,t_{n-j})}{\Im} \int_{j\Im}^{(j+1)\Im} \left(t_{j+1} - \eta\right)^{-\beta} d\eta, \\ &= \begin{cases} \frac{\Im^{-\beta}}{\Gamma(2-\beta)}(p^{n+1} - p^n) + \frac{\Im^{-\beta}}{\Gamma(2-\beta)} \sum\limits_{j=1}^{n} (p^{n+1-j} - p^{n-j})[(j+1)^{1-\beta} - j^{1-\beta}], & n \geq 1, \\ \frac{\Im^{-\beta}}{\Gamma(2-\beta)}(p^1 - p^0), & n = 0. \end{cases}\end{aligned}$$

Let $a_0 = \frac{\Im^{-\beta}}{\Gamma(2-\beta)}$ and $b_j = (j+1)^{1-\beta} - j^{1-\beta}$, $j = 0, 1, \ldots, n$. The above equation in a more precise form can be written as [41]

$$\frac{\partial^\beta p(v, t_{n+1})}{\partial t^\beta} = \begin{cases} a_0(p^{n+1} - p^n) + a_0 \sum\limits_{j=1}^{n} b_j (p^{n+1-j} - p^{n-j}), & n \geq 1, \\ a_0(p^1 - p^0), & n = 0. \end{cases} \tag{4.3}$$

5. Numerical results

Using linear and nonlinear PDEs, we validate the applicability, accuracy, and order of convergence of the proposed LRBFCM. The solved test problems are related to European and American options, with and without exact solutions . For accuracy measurements, we have used the maximum error (L_∞) and relative error (L_{rel}) norms and numerical rate of convergence (L_{cr}) in space:

$$\begin{aligned} L_\infty &= \max|p_{ex} - p|, \\ L_{rel} &= \left|(p_{ex} - p)/p_{ex}\right|, \end{aligned}$$

$$L_{cr} = \frac{\log_{10}\left(\|p_{ex} - p_{n_j}\|/\|p_{ex} - p_{n_{j+1}}\|\right)}{\log_{10}\left(n_j/n_{j+1}\right)},$$

where p_{ex} and p represent the exact and numerical values respectively. If the price of an option is particularly sensitive in one location, it makes sense to focus the mesh in that area. Adapting the grid around the option's strike price E may be advantageous.

$$v_j = E + \theta \sinh(d_1 \frac{j}{N} + d_2(1 - \frac{j}{N})), \quad j = 1, 2, ..., N,$$

where $d_1 = \sinh^{-1}((v_N - E)/\theta)$, $d_2 = \sinh^{-1}((v_o - E)/\theta)$, $\theta = 0.5, 5$.

Test Problem 5.1. *Consider a time-fractional model [7] with homogeneous boundary conditions*

$$\begin{aligned} &\frac{\partial^\beta p}{\partial t^\beta} = \frac{1}{2}\sigma^2 v^2 \frac{\partial^2 p}{\partial v^2} + rv\frac{\partial p}{\partial v} - rp + f(v,t), \quad (v,t) \in (0, v_{max}) \times (0, T), \\ &p(0,t) = 0, \quad p(v_{max}, t) = 0, \\ &p(v,0) = v^2(1-v), \end{aligned} \tag{5.1}$$

where

$$f = \left(\frac{2t^{2-\beta}}{\Gamma(3-\beta)} + \frac{2t^{1-\beta}}{\Gamma(2-\beta)}\right)v^2(1-v) - (t+1)^2[x(2-6v) + y(2v-3v^2) - zv^2(1-v)]$$

is chosen such that $p = (t+1)^2 v^2(1-v)$ is the exact solution of (5.1). The parameters in this problem are $r = 0.05, \sigma = 0.25, x = \frac{1}{2}\sigma^2, y = r - a, z = r$, $v_{max} = 1$ and $T = 1$.

Test Problem 5.2. *Consider a time-fractional model [7] with non-homogeneous boundary conditions*

$$\begin{aligned} &\frac{\partial^\beta p}{\partial t^\beta} = \frac{1}{2}\sigma^2 v^2 \frac{\partial^2 p}{\partial v^2} + rv\frac{\partial p}{\partial v} - rp + f(v,t), \quad (v,t) \in (0, v_{max}) \times (0, T), \\ &p(0,t) = (t+1)^2, \quad p(v_{max}, t) = 3(t+1)^2, \\ &p(v,0) = v^3 + v^2 + 1, \end{aligned} \tag{5.2}$$

where

$$f = \left(\frac{2t^{2-\beta}}{\Gamma(3-\beta)} + \frac{2t^{1-\beta}}{\Gamma(2-\beta)}\right)(v^3 + v^2 + 1) - (t+1)^2[x(6v+2) + y(3v^2+2v) - z(v^3+v^2+1)]$$

is utilized to ensure that $p = (t+1)^2(v^3 + v^2 + 1)$ yields the exact solution of (5.2). Values for the parameters are used here as $r = 0.5, x = 1, y = r - a, z = r, v_{max} = 1$ and $T = 1$.

Figures 1 and 2 respectively, illustrate the rates of convergence and slopes of the time-fractional models (5.1) and (5.2). Figure 3 shows the numerical solution of (5.1) using $N = 64$ and $\beta = 0.7$, whereas Figure 4 shows the numerical solution of (5.2) using $N = 16$ and $\beta = 0.7$. The numerical results generated by the LRBFCM are in good agreement with the exact solutions and implicit discrete scheme (IDS) [7], as can be seen from the figures. The suggested LRBFCM's numerical results for Test Problem 5.1 for $N = 21$, $\beta = 0.7$, and various values of the shape parameter c are displayed in Figure 5 (left), along with the relevant condition numbers κ (right). One can observe from the figure

that the LRBFCM provides reliable and accurate results throughout a wide range i.e., $(0 - 500)$*, and that the numerical values are equivalent to those of the IDS [7]. The suggested approach is only slightly superior to the error norm of the IDS [7]. The reason is that the suggested approach is explicit and contains temporal step-size restrictions, whereas the implicit scheme does not have such restrictions.*

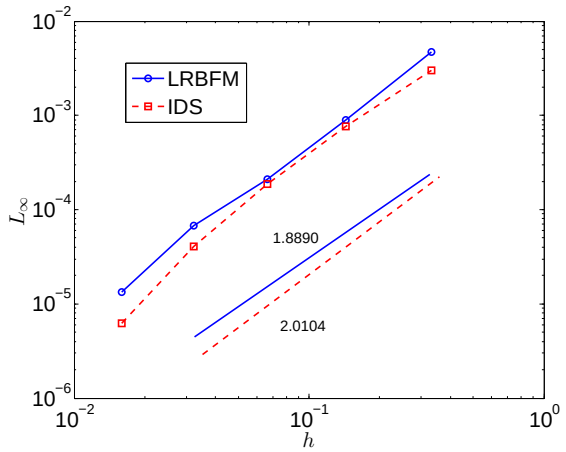

Figure 1. L_∞ error at various h values for Test Problem 5.1 using the LRBFCM and IDS [7].

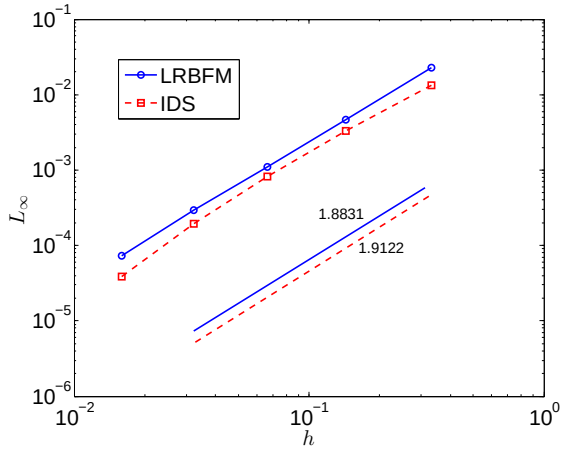

Figure 2. L_∞ error at various h values for Test Problem 5.2 using the LRBFCM and IDS [7].

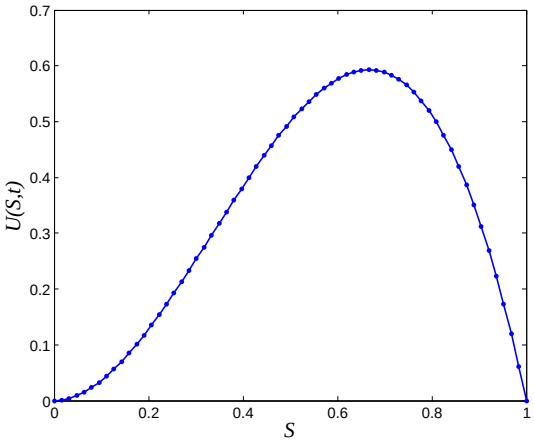

Figure 3. Numerical solution of the LRBFCM for Test Problem 5.1 using $N = 64$, $\beta = 0.7$ and $T = 1$.

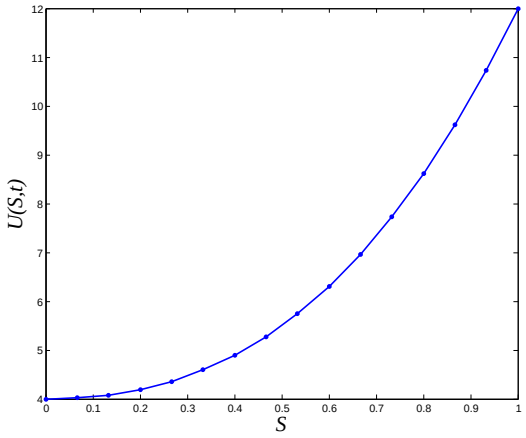

Figure 4. Numerical solution of the LRBFCM for Test Problem 5.2 using $N = 16$, $\beta = 0.7$ and $T = 1$.

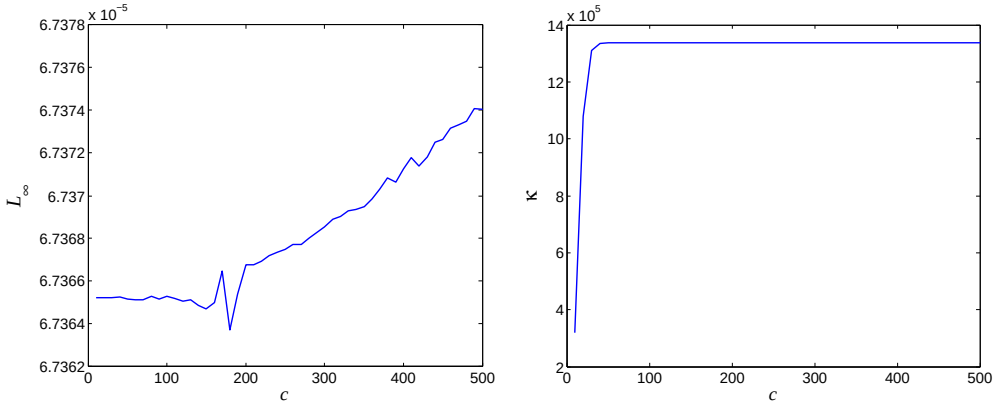

Figure 5. (left) L_∞ versus shape parameter c; (right) condition number κ versus shape parameter c for Test Problem 5.1.

Test Problem 5.3. *Consider the following TFBSM [36] for European call options:*

$$\begin{aligned} &\frac{\partial^\beta p}{\partial t^\beta} = \frac{1}{2}\sigma^2 v^2 \frac{\partial^2 p}{\partial v^2} + rv\frac{\partial p}{\partial v} - rp, \quad (v,t) \in (0, v_{max}) \times (0,T), \\ &p(v,0) = \max(v - E, 0), \\ &p(0,t) = 0, \quad p(v_{max}, t) = v_{max} - Ee^{-rt}, \quad t \in (0,T) \end{aligned} \tag{5.3}$$

with $r = 0.04, \sigma = 0.3, E = 10, v_{max} = 40$ *and* $T = 1$.

Since there is no exact solution for (5.3) the error norm is approximated using the double mesh approach. Table 1 compares L_∞ *error and convergence rates using the LRBFCM and the CDM [36]. Using* $\beta = 0.7$ *and* $N = 41$*, Figure 6 illustrates the numerical solution of a European call option. Figure 7 shows the volatility value (*$\sigma = 0.3$*) to display the price of a European call option for various* β *values at the out-of-the-money (OTM), at-the-money (ATM), and in-the-money (ITM) positions. We have modified the volatility value to compare the TFBSM's contribution to that of the classical BS model, and we discover that, in the case of European call options, changing the volatility values can affect the outcomes. The numerical outcomes of the TFBSM are somewhat superior to those produced by the conventional BS (*$\beta = 1$*) when the volatility* $\sigma < 0.43$*, and comparably better values are achieved for the call option. The numerical output of the classical BS (*$\beta = 1$*) model performs just slightly better than that of the TFBSM when the volatility* $\sigma \geq 0.43$*. (see Figures 8 and 9). Figure 10 displays the cost of the European call option for* $\beta = 0.7$ *and* $N = 50$ *given uniform nodes (left) and non-uniform nodes (right). Figure 11 depicts a detailed comparison of European call option prices for uniform and non-uniform nodes. Figure 11 illustrates that a non-uniform grid can provide a somewhat reasonable pricing. Despite the suggested technique being more explicit and cost-effective than the CDM [36], it is evident from the assessment that its performance is equivalent to that of the CDM [36].*

Table 1. Comparison of L_∞ and convergence rates (L_{rel}) for various uniform nodes and β values for Test Problem 5.3.

	$N = 64$		$N = 128$		$N = 256$		$N = 512$	
β	CDM [36]	LRBFCM	CDM [36]	LRBFCM	CDM [36]	LRBFCM	CDM [36]	LRBFCM
0.1	1.2029e−3	3.7775e−3	2.9366e−4	9.4820e−4	7.2309e−5	2.2235e−4	1.7939e−5	5.0526e−5
	2.03	1.99	2.02	2.09	2.01	2.14	-	-
0.3	1.1477e−3	3.6010e−3	2.7890e−4	9.0293e−4	6.8796e−5	2.2586e−4	1.7077e−5	5.3165e−5
	2.04	2.00	2.02	2.00	2.01	2.09	-	-
0.5	1.0952e−3	3.4144e−3	2.6816e−4	8.5492e−4	6.1627e−5	2.1359e−4	1.6437e−5	5.1588e−5
	2.03	2.00	2.02	2.00	2.01	2.05	-	-
0.7	1.0831e−3	3.2257e−3	2.6511e−4	8.0467e−4	6.5542e−5	2.0029e−4	1.6287e−5	4.4524e−5
	2.03	2.00	2.02	2.01	2.01	2.17	-	-
0.9	1.1384e−3	3.0512e−3	2.7875e−4	7.7231e−4	6.8869e−5	1.7356e−4	1.7125e−5	3.9350e−5
	2.03	1.98	2.02	2.15	2.01	2.14	-	-

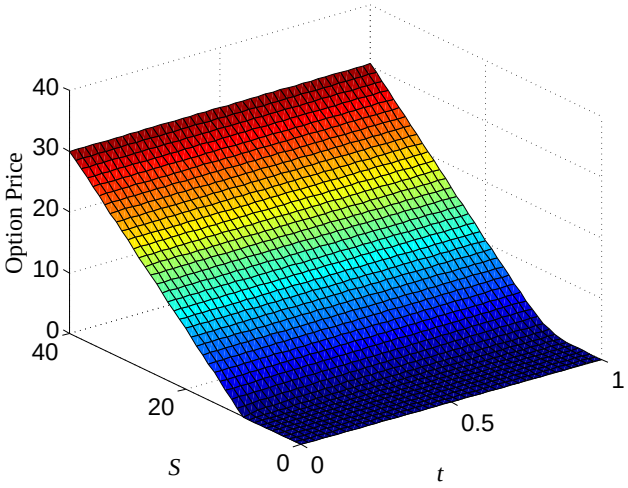

Figure 6. 3D view of European call option pricing for Test Problem 5.3 at $N = 41$ and $\beta = 0.7$.

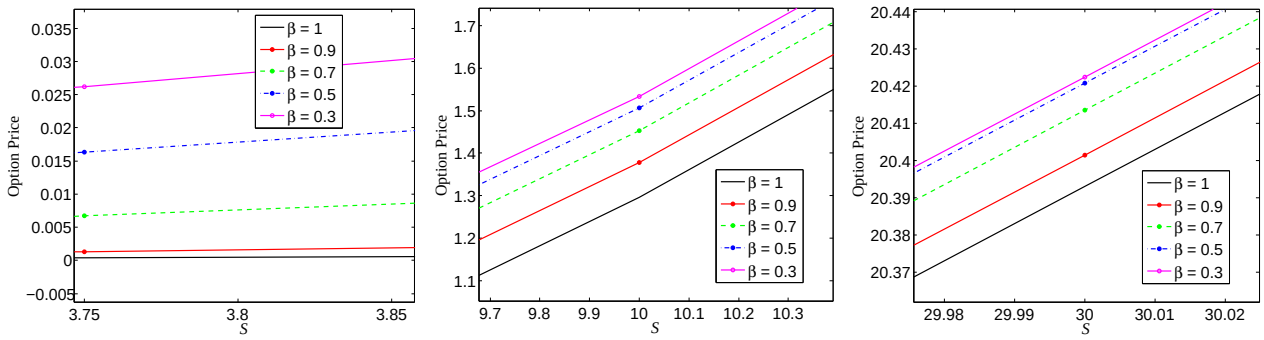

Figure 7. Numerical solutions of European call option pricing for Test Problem 5.3 for different values of β under conditions of OTM (left), ATM (center), ITM (right).

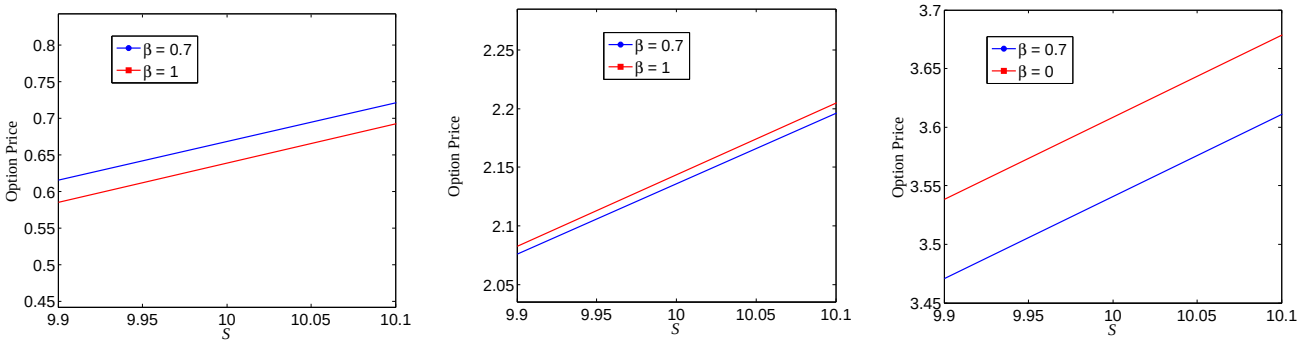

Figure 8. Evaluation of European call option pricing for Test Problem 5.3 for various volatility values ($\sigma = 0.1, 0.5, 0.9$) at ATM.

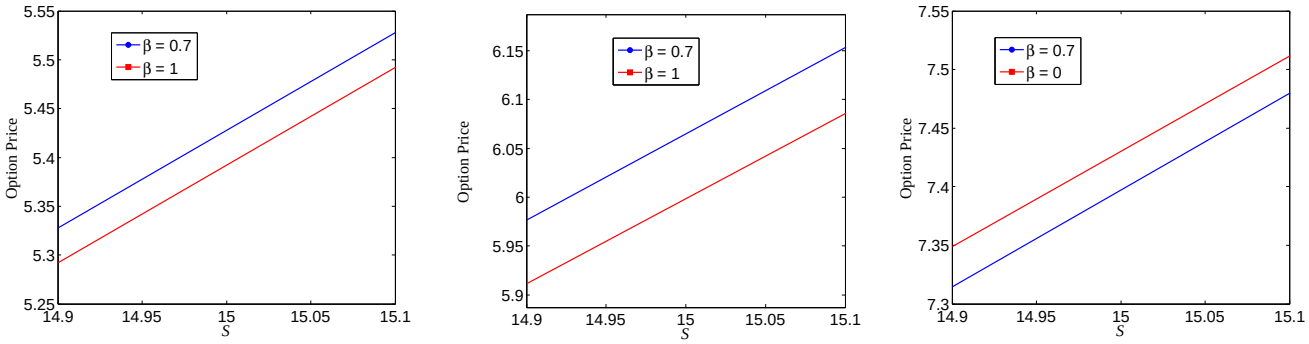

Figure 9. Evaluation of European call option pricing for Test Problem 5.3 for various volatility values ($\sigma = 0.1, 0.5, 0.9$) at ITM.

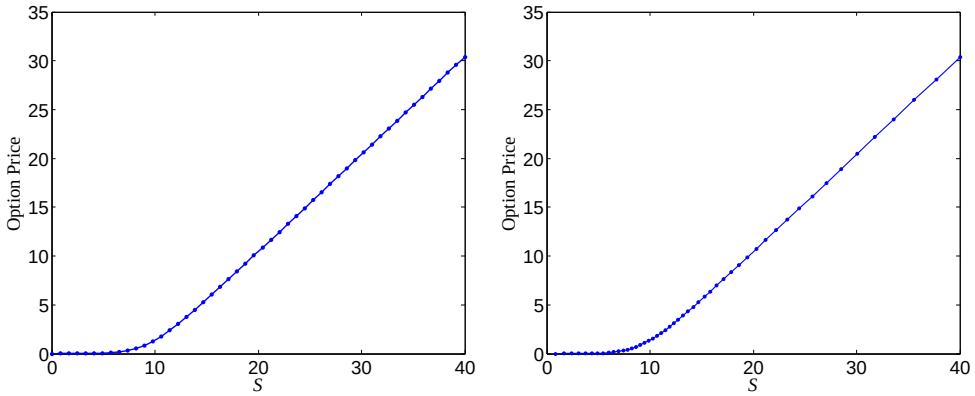

Figure 10. Numerical solution obtained using uniform (left) and non-uniform (right) nodes for European call option pricing for Test Problem 5.3 at $N = 50, \beta = 0.7$ and $T = 1$.

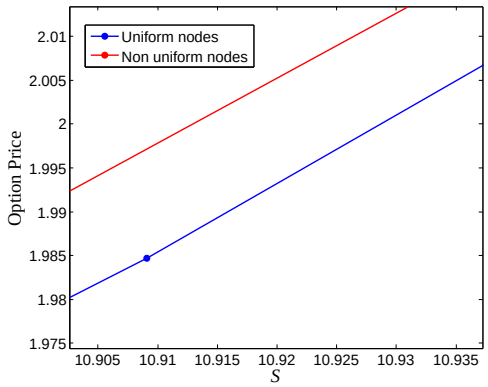

Figure 11. A close view of uniform and non-uniform node numerical solution for European call option pricing for Test Problem 5.3 at $N = 50, \beta = 0.7$ and $T = 1$.

Test Problem 5.4. *Consider the nonlinear TFBSM [13] under the condition of a transaction cost*

$$\frac{\partial^\beta p}{\partial t^\beta} + rv\frac{\partial p}{\partial v} + \frac{1}{2}\sigma^2 v^2\left(1 + 2\rho v\frac{\partial^2 p}{\partial v^2}\right)\frac{\partial^2 p}{\partial v^2} - rp = 0, \quad (v,t) \in (0, v_{max}) \times (0,T), \tag{5.4}$$

subject to

$$p(v,0) = \max\left(v - \rho^{-1}\left(\sqrt{v_o v + \frac{v_o}{4}}\right), 0\right),$$

where the market liquidity is ρ and initial stock price is v_o. The exact solution of this equation is

$$p(v,t) = v - \rho^{-1}\sqrt{v_o}\left[\sqrt{v}\exp\left(\frac{r+\frac{\sigma^2}{4}}{2}\right)t + \frac{\sqrt{v_o}}{4}\exp\left(r+\frac{\sigma^2}{4}\right)t\right]. \tag{5.5}$$

For purposes of numerical illustration, we take into account the parameters $|\rho| = 0.01$, $r = 0.06$, $\sigma = 0.4$, $v_o = 4$ and various v and β values. Tables 2 and 3 compare relative errors and also show the computational time for the proposed LRBFCM while Figures 12 and 13 compare numerical estimates for $\beta = 1$ and $\beta = 0.5$, respectively. Figure 13 (right) demonstrates that the MDTM [13] diverges while the LRBFCM yields accurate and converging results. The tables and figures make it clear that the LRBFCM offers substantially better accuracy even for the nonlinear TFBSM when transaction costs are included.

Table 2. Comparison of numerical solutions and relative errors at $\beta = 1$ and $T = 0.5$ for Test Problem 5.4.

		MDTM [13]		LRBFCM	
v	*Exact*	p	L_{rel}	p	L_{rel}
0.5	250.6286	243.2212	0.029555	246.4610	0.0166286
1.0	311.1902	301.9564	0.029673	307.0002	0.0134642
1.5	357.7770	347.1821	0.029613	353.5727	0.0117511
2.0	397.1301	385.4947	0.029299	392.9138	0.0106167
2.5	431.8603	419.4882	0.028648	427.6335	0.0097873
3.0	463.3067	450.5316	0.027574	459.0704	0.0091436
3.5	492.2649	479.4798	0.025972	488.0199	0.0086234
4.0	519.2532	506.9340	0.023725	514.9999	0.0081909
4.5	544.6315	533.3594	0.020697	540.3707	0.0078233
Computational time of the LRBFCM = 0.46 seconds for N=50					

Table 3. Comparison of numerical solutions and relative errors at $\beta = 0.5$ and $T = 0.5$ for Test Problem 5.4.

		MDTM [13]		LRBFCM	
v	*Exact*	p	L_{rel}	p	L_{rel}
0.02	134.1475	131.455	0.020071	128.9427	0.0387987
0.04	146.1798	143.0975	0.021086	142.9939	0.0217936
0.06	155.4171	152.0336	0.021770	152.0159	0.0218846
0.08	163.2077	159.5681	0.022300	159.7693	0.0210674
0.10	170.0738	166.2063	0.022740	166.6394	0.0201933
1.0	311.1901	-	-	308.5197	0.0085813
2.0	397.1300	-	-	394.9583	0.0054686
3.0	463.3067	-	-	461.5175	0.0038618
Computational time of the LRBFCM = 0.71 seconds for N=400					

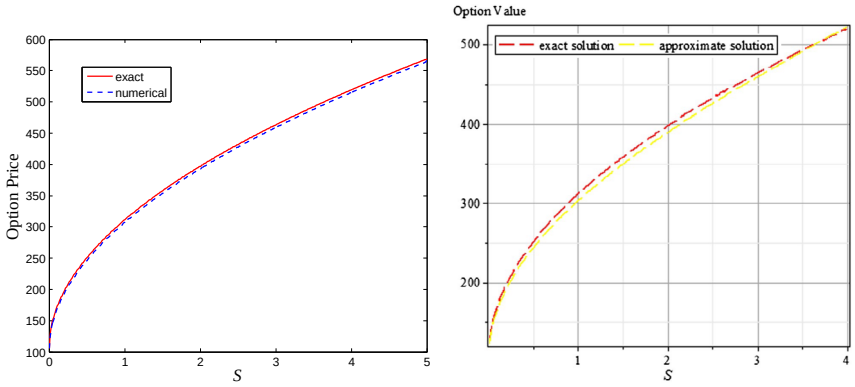

Figure 12. Numerical solution for Test Problem 5.4 using the LRBFCM (left) and MDTM (right) at $T = 0.5$ and $\beta = 1$.

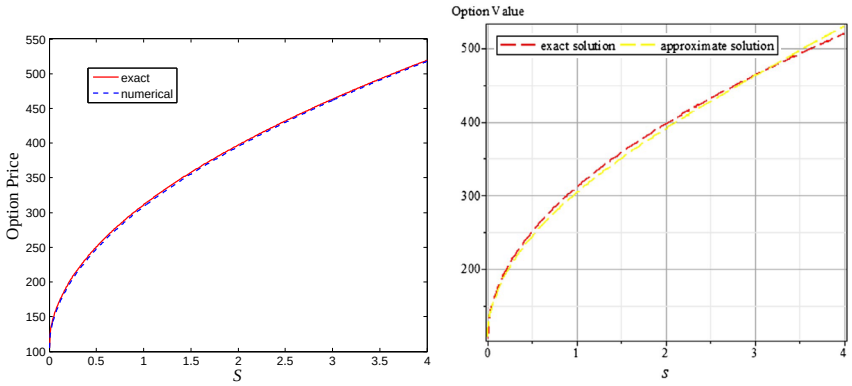

Figure 13. Numerical solution for Test Problem 5.4 using the LRBFCM (left) and MDTM (right) at $T = 0.5$ and $\beta = 0.5$.

Test Problem 5.5. *Consider the following TFBSM for American put options using the penalty term approach*

$$\begin{aligned} &\frac{\partial^\beta p}{\partial t^\beta} = \frac{1}{2}\sigma^2 v^2 \frac{\partial^2 p}{\partial v^2} + rv\frac{\partial p}{\partial v} - rp + \frac{\mu C}{p + \mu - q(v)}, \quad (v,t) \in (0, v_{max}) \times (0,T), \\ &p(v,0) = \max(E - v, 0), \\ &p(0,t) = E, \quad p(v_{max}, t) = 0, \quad t \in (0,T) \end{aligned} \tag{5.6}$$

with parameters $\sigma = 0.2, r = 0.1, E = 1, \mu = 0.01, C = rE, q(v) = E - v, v_{max} = 2$ *and* $T = 1$.

The exact solution of the PDE (5.6) is not available. Therefore, to estimate the errors, we applied the double mesh principle. Table 4 compares the reference price [38] to the results of the integer order model ($\beta = 1$*) and existing methods [38, 39]. In fact, when* $\beta = 1$*, the suggested approach resembles [38, 39]. Table 5 provides the numerical solution for numerous values of N and* β*. The rates of convergence and corresponding slopes are shown in Figure 14. The surface plot of an American put option with* $\beta = 0.5$ *and* $N = 21$ *is shown in Figure 15. Figure 16 illustrates the pricing of an American put option at ITM (left), ATM (middle) and OTM for various levels of* β *under the condition of volatility (*$\sigma = 0.2$*). The figure shows that the value of the put option decreases as the value of* β *decreases. When volatility is increased for the American put option from 0.1 to 0.9, the TFBSM numerical results become better than those of the traditional BS (*$\beta = 1$*) (see Figures 17 and 18). Therefore, we draw the conclusion that, in comparison to the traditional BS procedure, the TFBSM can more precisely capture physical features like a jump or significant movement. As illustrated in Figure 19, the price of an American put option has also been determined for uniform nodes (left) and non-uniform nodes (right). Figure 20 displays a close view of the uniform and non-uniform grids used to compare the prices of American put options. Figure 20 shows that we can get a rather reasonable pricing on a non-uniform grid.*

Table 4. Comparison of exact and approximate solutions at $T = 1$ and $\beta = 1$ values for Test Problem 5.5.

v	Reference price [38]	LRBFCM	[38]	[39]
0.6	0.4000037	0.4000043	0.4000176	0.4000185
0.7	0.3001161	0.3001216	0.3001007	0.3002333
0.8	0.2020397	0.2020324	0.2019901	0.2022428
0.9	0.1169591	0.1168272	0.1165422	0.1154885
1.0	0.0602833	0.0601380	0.0597033	0.0580422
1.1	0.0293272	0.0292004	0.0287648	0.0276763
1.2	0.0140864	0.0140160	0.0136840	0.0132349
1.3	0.0070408	0.0070086	0.0068192	0.0066983
1.4	0.0038609	0.0038484	0.0037485	0.0037539

Table 5. L_∞ at various uniform nodes and β values for Test Problem 5.5.

N	21	41	81	161
$\beta = 0.9$	5.7315e−3	8.3826e−4	1.6169e−4	4.7204e−5
$\beta = 0.7$	5.8620e−3	1.1410e−3	2.3723e−4	2.0000e−4
$\beta = 0.5$	6.0068e−3	1.3576e−3	7.5219e−4	5.6710e−4
$\beta = 0.3$	2.3432e−3	2.5194e−3	1.5109e−3	6.7021e−4

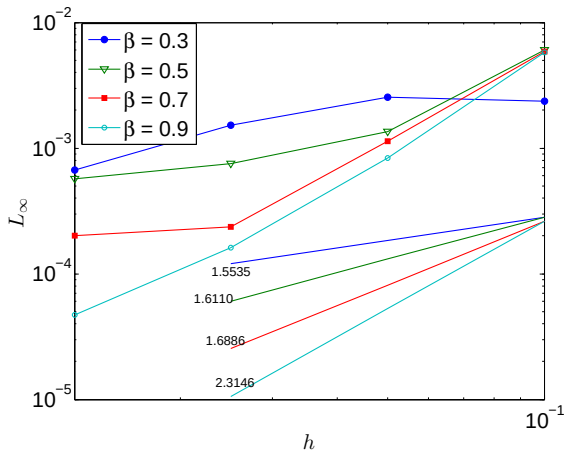

Figure 14. L_∞ error at various values of h and β for Test Problem 5.5 using the LRBFCM.

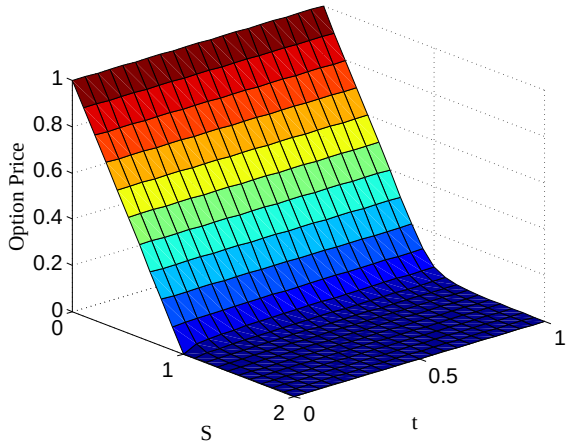

Figure 15. 3D view of American put option pricing for Test Problem 5.5 at $N = 21$ and $\beta = 0.5$.

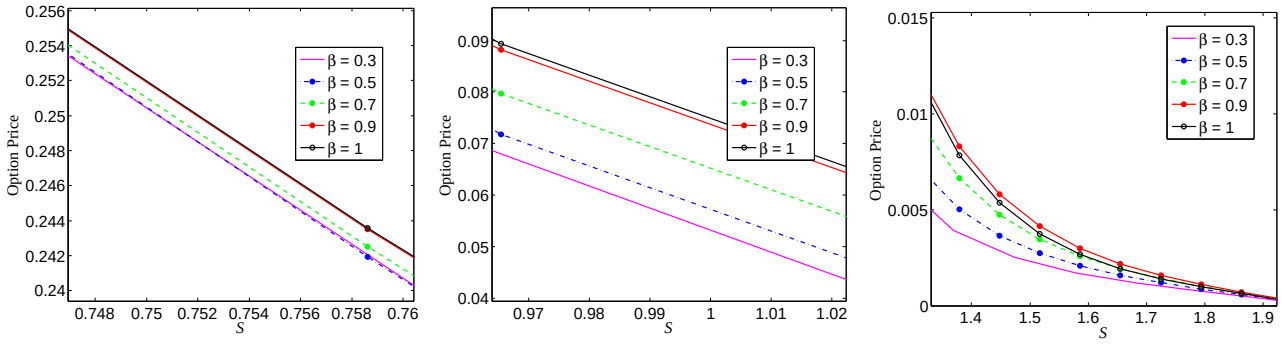

Figure 16. Numerical solution of American put option pricing for Test Problem 5.5 for different values of β, ITM (left), ATM (center), OTM (right).

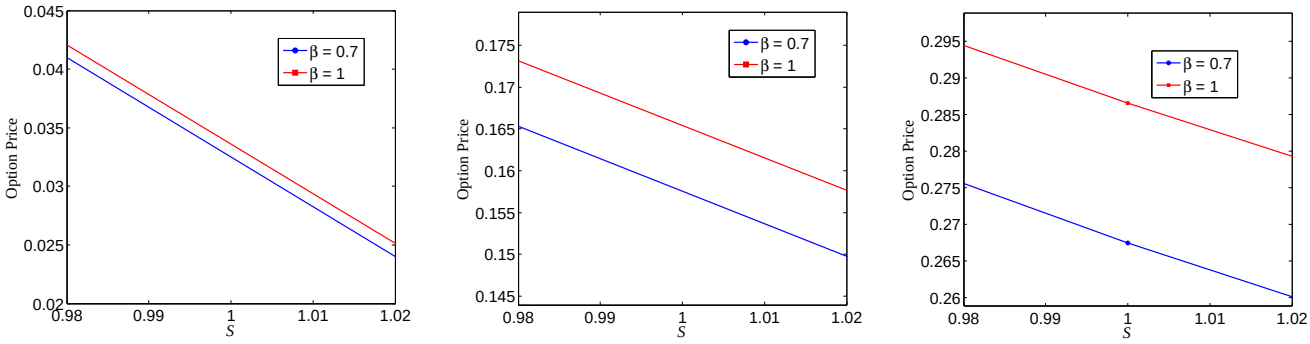

Figure 17. Evaluation of European call option pricing for Test Problem 5.5 for various volatility values ($\sigma = 0.1, 0.5, 0.9$) at ATM.

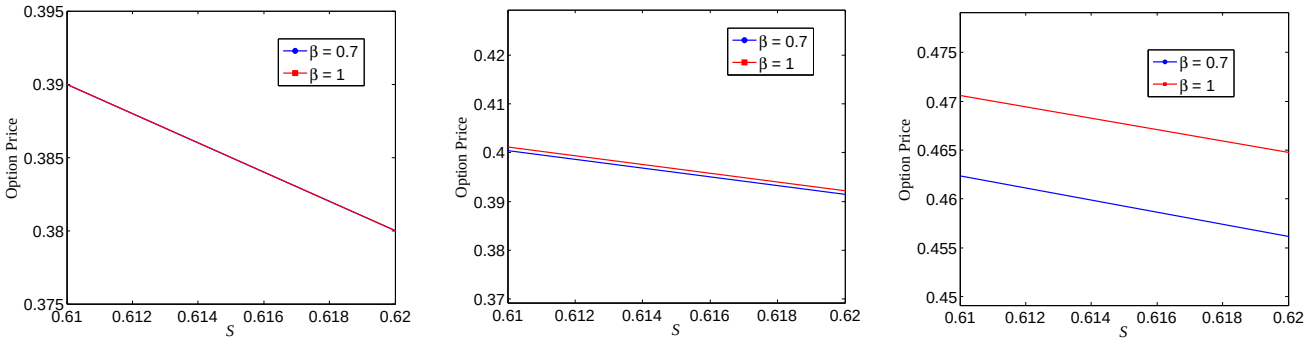

Figure 18. Evaluation of American put option pricing for Test Problem 5.5 for various volatility values ($\sigma = 0.1, 0.5, 0.9$) at ITM.

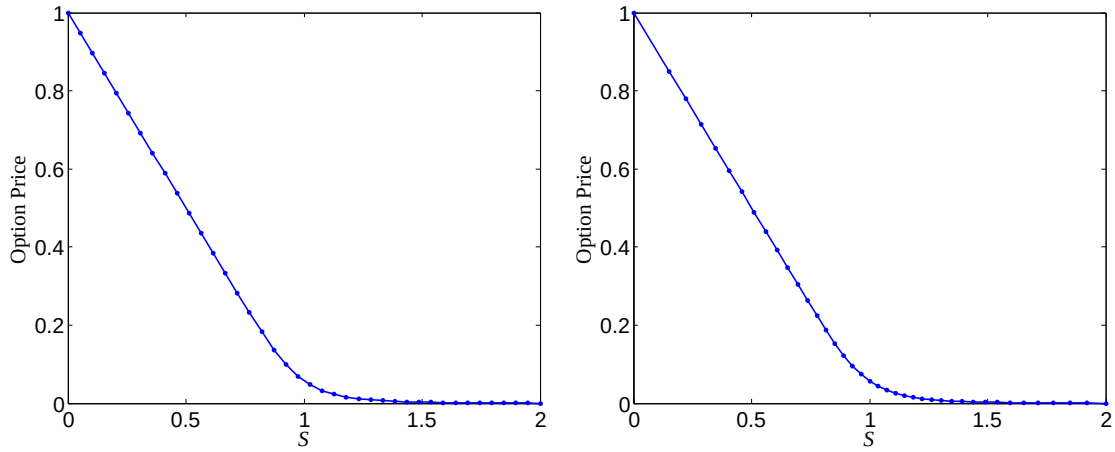

Figure 19. Numerical solution under the conditions of uniform (left) and non-uniform (right) nodes for American put option pricing for Test Problem 5.5 at $\beta = 0.5$ and $T = 1$.

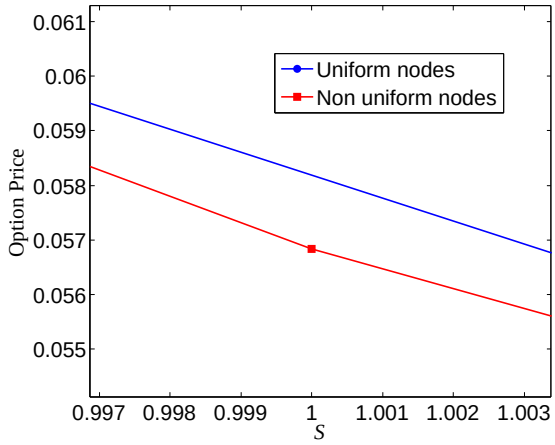

Figure 20. A close view of uniform and non-uniform node numerical solutions for American put option pricing for Test Problem 5.5 at $\beta = 0.7$ and $T = 1$.

6. Conclusions

The paper presents a successful solution to the the TFBSM for both European and American options, as well as a nonlinear time-fractional model for an illiquid market with transaction costs, using the proposed method of the LRBFCM. The LRBFCM combines a polynomial component with an RBF component, resulting in improved accuracy and stability of the function approximation. The polynomial component captures the overall behavior of the function, while the RBF component focuses on local features. This method has the potential to be applied to various fractional BS models, as well as other PDE problems in finance and other fields that involve fractional derivatives.

We have observed the following value additions during numerical experimentation

- To compare the TFBSM's advantages over the classical BS model for call and put options, numerical experiments were performed for various β values.

- It has been observed that the change in volatility can influence the end results. We have observed that the TFBSM's numerical outcome for call options, when the volatility $\sigma < 0.43$, is substantially better than that of the classical BS model ($\beta = 1$).
- The TFBSM performs better than the classical BS model when the volatility for put options is raised from 0.1 to 0.9.
- Call and put option strike prices estimated on non-uniform nodes are higher than those calculated on uniform nodes.
- When compared to the classical BS technique, the TFBSM can more correctly capture physical features such as large movements or jumps.
- Numerical results of the explicit LRBFCM are comparable for the reported implicit methods.
- In some circumstances, the performance of the LRBFCM is proven to be more efficient and accurate than current approaches in the literature.
- The numerical approach of the LRBFCM is reliable and practical when applied to fractional PDEs, as evidenced by the numerical results of the numerous option pricing models that were solved using it.

Use of AI tools declaration

The authors declare they have not used Artificial Intelligence (AI) tools in the creation of this article.

Acknowledgments

This research work was funded by Institutional Fund Projects under grant no. (IFPIP: 1582-130-1443). The authors gratefully acknowledge the technical and financial support provided by the Ministry of Education and King Abdulaziz University, DSR, Jeddah, Saudi Arabia

Conflict of interest

The authors declare that there is no conflict of interests regarding the publication of this paper.

References

1. F. Black, M. Scholes, The pricing of options and corporate liabilities, *J. Pol. Econ.*, **81** (1973), 637–654. https://doi.org/10.1086/260062
2. P. Carr, L. Wu, The finite moment log stable process and option pricing, *J. Finance*, **58** (2003), 753–777. https://doi.org/10.1111/1540-6261.00544
3. A. Farhadi, M. Salehi, G. Erjaee, A new version of Black-Scholes equation presented by time-fractional derivative, *Iran. J. Sci. Technol. Trans. Sci.*, **42** (2018), 2159–2166. https://doi.org/10.1007/s40995-017-0244-7
4. G. Jumarie, Derivation and solutions of some fractional Black-Scholes equations in coarse-grained space and time. Application to Merton's optimal portfolio, *Comput. Math. Appl.*, **59** (2010), 1142–1164. https://doi.org/10.1016/j.camwa.2009.05.015

5. A. Cartea, D. del-Castillo-Negrete, Fractional diffusion models of option prices in markets with jumps, *Physica A*, **374** (2007), 749–763. https://doi.org/10.1016/j.physa.2006.08.071
6. J. R. Liang, J. Wang, W. J. Zhang, W. Y. Qiu, F. Y. Ren, The solution to a bi-fractional Black-Scholes-Merton differential equation, *Int. J. Pure Appl. Math.*, **58** (2010), 99–112.
7. H. Zhang, F. Liu, I. Turner, Q. Yang, Numerical solution of the time fractional Black-Scholes model governing European options, *Comput. Math. Appl.*, **71** (2016), 1772–1783. https://doi.org/10.1016/j.camwa.2016.02.007
8. N. Özdemir, M. Yavuz, Numerical solution of fractional Black-Scholes equation by using the multivariate padé approximation, *Acta Phys. Pol.*, **132** (2017), 1050–1053. https://hdl.handle.net/20.500.12462/6405
9. Z. Cen, J. Huang, A. Xu, A. Le, Numerical approximation of a time fractional Black-Scholes equation, *Comput. Math. Appl.*, **75** (2018), 2874–2887. https://doi.org/10.1016/j.camwa.2018.01.016
10. W. Chen, X. Xu, S. P. Zhu, A predictor-corrector approach for pricing American options under the finite moment log-stable model, *Appl. Numer. Math.*, **97** (2015), 15–29. https://doi.org/10.1016/j.apnum.2015.06.004
11. W. Chen, S. Wang, A penalty method for a fractional order parabolic variational inequality governing American put option valuation, *Comput. Math. Appl.*, **67** (2014), 77–90. https://doi.org/10.1016/j.camwa.2013.10.007
12. R. Company, L. Jódar, J. R. Pintos, A numerical method for European option pricing with transaction costs nonlinear equation, *Math. Comput. Model.*, **50** (2009), 910–920. https://doi.org/10.1016/j.mcm.2009.05.019
13. S. O. Edeki, O. O. Ugbebor, E. A. Owoloko, Analytical solutions of a time-fractional nonlinear transaction-cost model for stock option valuation in an illiquid market setting driven by a relaxed Black-Scholes assumption, *Cogent Math.*, **4** (2017), 1352118. https://doi.org/10.1080/23311835.2017.1352118
14. Y. Chen, L. Wei, S. Cao, F. Liu, Y. Yang, Y. Cheng, Numerical solving for generalized Black-Scholes-Merton model with neural finite element method, *Digit. Signal Process.*, **131** (2022), 103757. https://doi.org/10.1016/j.dsp.2022.103757
15. Y. Chen, Y. Li, M. Wu, F. Lu, M. Hou, Y. Yin, Differentiating Crohn's disease from intestinal tuberculosis using a fusion correlation neural network, *Knowl. Based Syst.*, **244** (2022), 108570. https://doi.org/10.1016/j.knosys.2022.108570
16. T. Muhammad, H. Ahmad, U. Farooq, A. Akgül, Computational investigation of magnetohydrodynamics boundary of Maxwell fluid across nanoparticle-filled sheet, *Al-Salam J. Eng. Technol.*, **2** (2023), 88–97. https://doi.org/10.55145/ajest.2023.02.02.011
17. I. Ahmad, H. Ahmad, M. Inc, S. W. Yao, B. Almohsen, Application of local meshless method for the solution of two term time fractional-order multi-dimensional PDE arising in heat and mass transfer, *Therm. Sci.*, **24** (2020), 95–105. https://doi.org/10.2298/TSCI20S1095A

18. M. Nawaz, I. Ahmad, H. Ahmad, A radial basis function collocation method for space-dependent inverse heat problems, *J. Appl. Comput. Mech.*, **6** (2020), 1187–1199. https://doi.org/10.22055/JACM.2020.32999.2123

19. M. N. Khan, I. Ahmad, A. Akgül, H. Ahmad, P. Thounthong, Numerical solution of time-fractional coupled Korteweg-de Vries and Klein-Gordon equations by local meshless method, *Pramana*, **95** (2021), 6. https://doi.org/10.1007/s12043-020-02025-5

20. C. Piret, E. Hanert, A radial basis functions method for fractional diffusion equations, *J. Comput. Phys.*, **238** (2013), 71–81. https://doi.org/10.1016/j.jcp.2012.10.041

21. V. R. Hosseini, W. Chen, Z. Avazzadeh, Numerical solution of fractional telegraph equation by using radial basis functions, *Eng. Anal. Bound. Elem.*, **38** (2014), 31–39. https://doi.org/10.1016/j.enganabound.2013.10.009

22. H. R. Ghehsareh, S. H. Bateni, A. Zaghian, A meshfree method based on the radial basis functions for solution of two-dimensional fractional evolution equation, *Eng. Anal. Bound. Elem.*, **61** (2015), 52–60. https://doi.org/10.1016/j.enganabound.2015.06.009

23. A. Kumar, A. Bhardwaj, B. R. Kumar, A meshless local collocation method for time fractional diffusion wave equation, *Comput. Math. Appl.*, **78** (2019), 1851–1861. https://doi.org/10.1016/j.camwa.2019.03.027

24. M. Dehghan, M. Abbaszadeh, A. Mohebbi, An implicit RBF meshless approach for solving the time fractional nonlinear Sine-Gordon and Klein-Gordon equations, *Eng. Anal. Bound. Elem.*, **50** (2015), 412–434. https://doi.org/10.1016/j.enganabound.2014.09.008

25. A. Mohebbi, M. Abbaszadeh, M. Dehghan, The use of a meshless technique based on collocation and radial basis functions for solving the time fractional nonlinear Schrödinger equation arising in quantum mechanics, *Eng. Anal. Bound. Elem.*, **37** (2013), 475–485. https://doi.org/10.1016/j.enganabound.2012.12.002

26. A. Mohebbi, M. Abbaszadeh, M. Dehghan, Solution of two-dimensional modified anomalous fractional sub-diffusion equation via radial basis functions (RBF) meshless method, *Eng. Anal. Bound. Elem.*, **38** (2014), 72–82. https://doi.org/10.1016/j.enganabound.2013.09.015

27. S. Wei, W. Chen, Y. C. Hon, Implicit local radial basis function method for solving two-dimensional time fractional diffusion equations, *Therm. Sci.*, **19** (2015), 59–67. https://doi.org/10.2298/TSCI15S1S59W

28. M. Aslefallah, E. Shivanian, Nonlinear fractional integro-differential reaction-diffusion equation via radial basis functions, *Eur. Phys. J. Plus*, **130** (2015), 47. https://doi.org/10.1140/epjp/i2015-15047-y

29. S. Wei, W. Chen, Y. Zhang, H. Wei, R. M. Garrard, A local radial basis function collocation method to solve the variable-order time fractional diffusion equation in a two-dimensional irregular domain, *Numer. Methods Partial. Differ. Equ.*, **34** (2018), 1209–1223. https://doi.org/10.1002/num.22253

30. Z. Avazzadeh, V. Hosseini, W. Chen, Radial basis functions and FDM for solving fractional diffusion-wave equation, *Iran. J. Sci. Technol. Trans. Sci.*, **38** (2014), 205–212. https://doi.org/10.22099/IJSTS.2014.2260

31. A. Golbabai, O. Nikan, T. Nikazad, Numerical analysis of time fractional Black-Scholes European option pricing model arising in financial market, *Comput. Appl. Math.*, **38** (2019), 173. https://doi.org/10.1007/s40314-019-0957-7

32. P. K. Mishra, S. K. Nath, M. K. Sen, G. E. Fasshauer, Hybrid Gaussian-cubic radial basis functions for scattered data interpolation, *Comput. Geosci.*, **22** (2018), 1203–1218. https://doi.org/10.1007/s10596-018-9747-3

33. G. Jumarie, Stock exchange fractional dynamics defined as fractional exponential growth driven by (usual) Gaussian white noise. Application to fractional Black-Scholes equations, *Insur. Math. Econ.*, **42** (2008), 271–287. https://doi.org/10.1016/j.insmatheco.2007.03.001

34. M. Caputo, Linear models of dissipation whose Q is almost frequency independent-II, *Geophys. J. Int.*, **13** (1967), 529–539. https://doi.org/10.1111/j.1365-246X.1967.tb02303.x

35. W. Chen, X. Xu, S. P. Zhu, Analytically pricing double barrier options based on a time-fractional Black-Scholes equation, *Comput. Math. Appl.*, **69** (2015), 1407–1419. https://doi.org/10.1016/j.camwa.2015.03.025

36. Z. Cen, H. Jian, X. Aimin, L. Anbo, Numerical approximation of a time-fractional Black-Scholes equation, *Comput. Math. Appl.*, **75** (2018), 2874–2887. https://doi.org/10.1016/j.camwa.2018.01.016

37. A. Khaliq, D. Voss, S. Kazmi, A linearly implicit predictor-corrector scheme for pricing American options using a penalty method approach, *J. Bank. Financ.*, **30** (2006), 489–502. https://doi.org/10.1016/j.jbankfin.2005.04.017

38. G. E. Fasshauer, A. Q. M. Khaliq, D. A. Voss, Using meshfree approximation for multi-asset American option problems, *J. Chin. Inst. Eng.*, **27** (2004), 56. https://doi.org/10.1080/02533839.2004.9670904

39. M. K. Kadalbajooa, A. Kumar, L. Tripathia, Application of local radial basis function based finite difference method for American option problems, *Int. J. Comput. Math.*, **8** (2016), 1608–1624. https://doi.org/10.1080/00207160.2014.950571

40. S. A. Sarra, A local radial basis function method for advection-diffusion-reaction equations on complexly shaped domains, *Appl. Math. Comput.*, **218** (2012), 9853–9865. https://doi.org/10.1016/j.amc.2012.03.062

41. A. Yokuş, Comparison of caputo and conformable derivatives for time-fractional korteweg-de vries equation via the finite difference method, *Int. J. Mod. Phys. B*, **32** (2018), 1850365. https://doi.org/10.1142/S0217979218503654

AIMS Press